High Speed Solid Rotor Permanent Magnet Machines: Concept and Design

Puvan Arumugam, *member, IEEE,* Zuyuan Xu, Antonino La Rocca, Gaurang Vakil, Matthew Dickinson, Amankwah Emmanuel, Tahar Hamiti, Serhiy Bozhko, *member, IEEE,* Chris Gerada, *member, IEEE,* Stephen Pickering

***Abstract*—This paper proposes a novel solid rotor topology for an Interior Permanent Magnet (IPM) machine, adopted in this case for an aircraft starter-generator design. The key challenge in the design is to satisfy two operating conditions which are: a high torque at start and a high speed at cruise. Conventional IPM topologies which are highly capable of extended field weakening are found to be limited at high speed due to structural constraints associated with the rotor material. To adopt the IPM concept for high speed operation, it is proposed to adopt a rotor constructed from semi-magnetic stainless steel, which has a higher yield strength than laminated silicon steel. To maintain minimal stress levels and also minimize the resultant eddy current losses due to the lack of laminations, different approaches are considered and studied. Finally, to achieve a better tradeoff between the structural and electromagnetic constraints, a novel slitted approach is implemented on the rotor. The proposed rotor topology is verified using electromagnetic, static structural and dynamic structural Finite Element (FE) analyses. An experiment is performed to confirm the feasibility of the proposed rotor. It is shown that the proposed solid rotor concept for an IPM fulfils the design requirements whilst satisfying the structural, thermal and magnetic limitations.**

***Index Terms*—More-electric; aircraft; high speed machines; permanent magnet; interior; starter-generator; structural; solid rotor**

I. Introduction

THE aircraft electrical power systems in next generation commercial aircraft are undergoing significant development. Future aircraft power systems are expected to be more fuel efficient and also simpler to service and maintain. The way towards this goal has been identified as a move towards "More-electric" systems by the replacement of hydraulic and pneumatic sources of power with electrical counterparts [1, 2]. This can lead to an increased reliance on electrical power for a range of primary functions including actuation, de-icing, cabin air-conditioning and engine start. A more electric power generation system plays a key role in this technology and the paper focuses on the design of a starter-generator for such systems. One of the challenges often encountered in the design of a starter-generator for aero-engines is the need to satisfy two fundamental functions, namely to energize the engines during start-up and to generate power during normal engine operation. In addition, it should provide [3, 4], high power density [5] and sufficient reliability [6, 7].

An Interior Permanent Magnet (IPM) machine with a wide constant power to speed ratio is considered to be ideal for such applications [8-12]. In addition to the high energy efficiency, the IPM offers a high power to volume ratio [8, 9, 13-17]. However, the operational speed of the IPM topology is significantly limited by the material yield strength due to centrifugal force acting on the rotor body. The amount of force generated in the rotor depends on body mass and the operating speed. Since high speed operation is required by the application, the remaining way to minimize this force is through downsizing the rotor mass. This, however, this will limit the electromagnetic performance of the machine as it reduces either the machine's length, the rotor diameter, or both.

In [18], high silicon content laminated steel which has considerably higher yield strength than the other laminated steel (e.g. non oriented silicon steels: M270-50A and M250-35A) was employed in the design to improve the operational speed. Although an improvement can be achieved, the operational speed of the machine is limited by material yield strength against the centrifugal forces acting on the machine. In [19], the design process has been done in such a way to find a fine balance between magnetic and structural limitations. To achieve both the required structural and magnetic performance, the power to volume ratio needs to be compromised. Recent studies show that the centrifugal force can be used to extend the field weakening capability by adding a spring loaded mechanism with flux barriers [20, 21], introducing a self-activated flux weakening device/floating

Manuscript received March 10, 2016; revised May 209, 2016; accepted July 4, 2016. This work was funded under the Seventh Framework Programme Joint Technology Initiatives – Theme Clean Sky. Project Code: JTI-CS-2011-1-ECO-02-009 Alternator with Active Power Rectification and Health Monitoring.

The Corresponding author is Puvan Arumugam who is currently with Force Engineering Ltd, Shepshed, UK (e-mail: puvan@force.co.uk).

Matthew Dickinson is with Force Engineering Ltd, Shepshed, UK (e-mail: matt@force.co.uk)

Tahar Hamiti is currently with VEDECOM, French Institute for Energy Transition, Versailles, France (e-mail: tahar.hamiti@vedecom.fr).

Z. Xu, A. La Rocca, G. Vakil, E. Amankwah, S. Bozhko, C. Gerada, S. Pickering are with the Power Electronics Machines and Control Group, Faculty of Engineering, The University of Nottingham, UK (e-mail: chris.gerada@nottingham.ac.uk)

particles [22], or varying the PM direction [23]. Although these can be solutions to extend the field weakening, this would not improve the power density or the structural capability of the machine. A way of improving the power density of PM machines for high speed applications while also maintaining the structural integrity is subject to investigation.

The main objective of this paper is to present a novel concept for an Interior Permanent Magnet (IPM) machine to overcome the electromagnetic and structural constraints of the target application. The application requirements and the initial design are presented in section II. Section III presents the proposed solid rotor solution for an IPM machine. To improve structural integrity and minimize eddy current losses, three different rotor design approaches are considered, namely: a combination of both laminations and solid steel, segmented solid steel, and slitted solid steel. A tradeoff study is carried out in Section IV. Section V presents detailed structural analysis of an optimized machine to limit the localized stress acting on the rotor body. Herein a novel design approach is proposed to overcome the structural limitation while also compromising efficiency against the starting requirements. In section VI, an experiment is performed to show the eddy current minimization through the proposed slitted approach in comparison with a solid rotor body. The challenges and limitations involved in the design and methods to overcome such issues are discussed.

II. Initial Design

The target application is to design a machine that acts as a starter and a generator which feeds into a 270V DC supply with a nominal power of 45 kW at 32krpm. Fig. 1 shows the required torque-speed characteristic. The machine runs as a motor during engine start and must supply constant torque from standstill to ω_{start}. Between ω_{start} to ω_{min} the machine provides a constant power to accelerate the engine. When the machine reaches ω_{min} it operates as a generator that generates a maximum power of 45 kW at a maximum speed (ω_{max}) of 32 krpm.

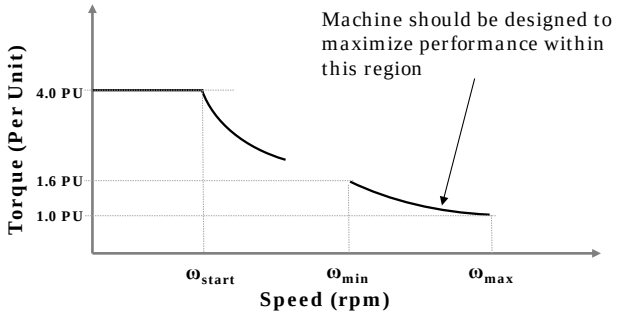

Fig. 1. Required torque-speed characteristic of the aircraft starter-generator

In the preliminary design, an IPM machine is designed to satisfy the electromagnetic requirements. To overcome the structural limitations, high silicon content (6.5%) electrical steel that has better mechanical properties and relatively poor magnetic properties has initially been adopted to allow a maximum stress of ~800 MPa. Nevertheless, it has been noted that although the designed machine is capable of extended field weakening, the stress limit still constitutes a bottleneck in reaching the maximum required speed of 32 krpm. Only 80% of the required maximum speed can be achieved while fulfilling the peak torque requirement.

III. Solid Rotor IPM machine

To overcome the structural limitations mentioned above and thus extend the operational speed required by the application, semi-magnetic stainless steel which has high yield strength limit and non-linear isotropic magnetic permeability (maximum flux density is ~1.4T) is therefore proposed. The advantages of having semi-magnetic stainless steel over laminated magnetic steel are:

- One solid body which has higher yield strength and higher stiffness (better rotor dynamic performance);
- Better thermal properties (lower thermal resistance in the axial direction);
- Semi-magnetic, however the bridges can easily be saturated.

The key disadvantage of semi-magnetic stainless steel is that the material has a relatively high electric conductivity and therefore it is subject to higher eddy current losses when compared to laminated silicon steel. This could be significantly minimized via a different structural adaptation. Within this study feasible structural adaptations are therefore considered. Two different rotor arrangements are implemented in place of a complete solid rotor body as shown Fig. 2a. Those are:

1. Segmented semi-magnetic stainless steel rotor yoke fitted onto a non-magnetic stainless steel shaft (Fig. 2b);
2. Circumferentially slitted /milled (around the outer rotor periphery) solid rotor body as shown in Fig. 2c.

The analysis of the abovementioned arrangements is presented via a trade-off study in section IV.

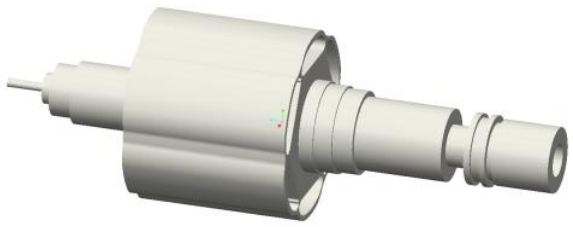

(a)

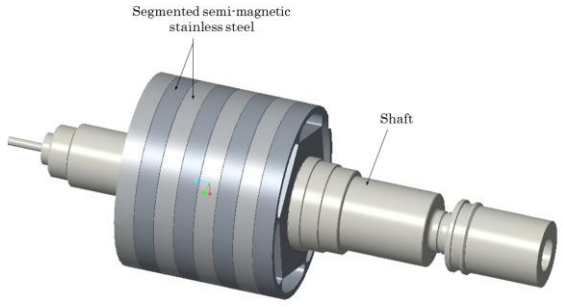

(b)

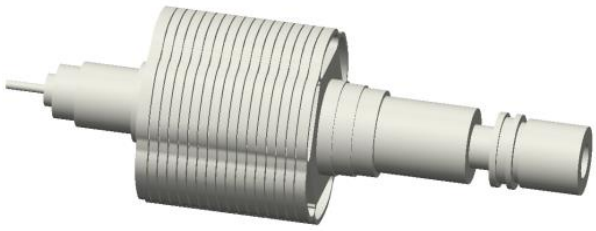

(c)

Fig. 2. IPM rotor with (a) unmodified solid rotor, (b) axially segmented rotor settled on stainless steel shaft and (c) circumferentially slitted/milled solid rotor

IV. Trade-off Study

By selecting a high strength and high stiffness material for the rotor, the limitation on the speed can be improved significantly. As previously mentioned, the main disadvantage of a solid rotor is the excessive eddy current losses. In order to minimize these losses, the rotor can be made of either segmented solid disks or a slitted single rotor body (see Fig.2c). Instead of using solid conductive iron for the segmented case, combinations of both high yield strength (~800MPa) silicon steel laminations and semi-magnetic stainless steel (see Fig.2b) as a hybrid concept could also be considered. In such an arrangement, it is expected that the solid steel delivers the structural capability to withstand the centrifugal force at high speed while the laminated steel lowers the losses. In this section, the structural limitations of such arrangements (the hybrid and the slitted/ milled rotor concept) are investigated. Throughout the analysis, the axial length of the rotor is kept the same. The magnets are considered as a segmented piece with respect to the arrangement of the rotor. Stresses in the magnet are constrained to 90% of the maximum allowable stress and thus, cracks within the magnets can be avoided.

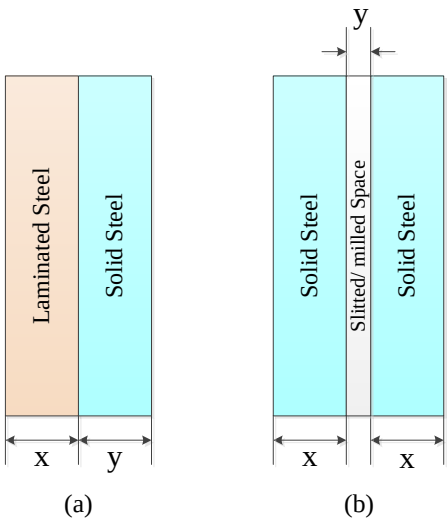

Fig. 3. Arrangement of the rotor with different segmentations (a) a combination of laminated steel and solid steel and (b) milled/slitted rotor with a space

Considering the fact that laminated steel reduces the losses effectively, an initial study is carried out for the combination of laminated steel and solid steel. In the analysis, a number of laminated steel and solid semi-magnetic stainless steel cases, which have a thickness of x mm and y mm respectively, and occupy the complete stack length of the rotor are considered. A solid thickness of 1mm, 2mm, 5mm and 10mm and an associated ratio of laminated steel from 50% to 550% with respect to solid steel are considered. The analysis is carried out using structural FE where an importance is given to the improvement on stress distribution within the entire structure by quantifying optimal thicknesses. The obtained maximum stress against the percentage variation of the laminated steel stack (x) with respect to solid steel (y) for different thicknesses of solid steel (see Fig.3a) is presented in Fig.4.

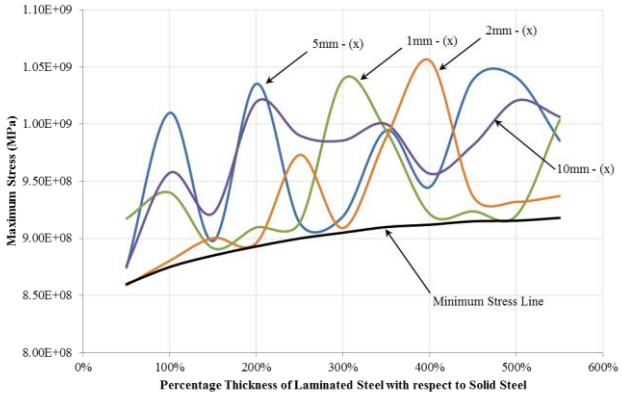

Fig. 4. Maximum stress occurring in laminated steel against percentage variation of the laminated steel stack (x) with respect to solid steel (y) for different thicknesses of solid steel

Fig.4 shows the obtained maximum stress distribution for different thicknesses of laminated steel with respect to the thickness of solid steel. For example, if the solid steel thickness considered is 1mm, the 250% of the laminated steel is 2.5mm. The results indicate how the stress varies in accordance with the selection of the material thickness and the optimum thickness ratio between solid steel to laminated steel which provides minimal stress.

From the minimum stress line in Fig.4, it can be seen that the stresses vary with the solid disk thickness. It also can be seen that the stress fluctuates as the thickness changes. This is mainly because of the maximum stress which occurs at different locations within the rotor with respect to changes in the material thickness. Between 50% and 300%, the stress reduction is significant and the most effective stress reduction for all the stack combinations (x+y) occurs at 1:2 ratios (150%) of x and y. However, the maximum stress is still higher than the yield strength of laminated steel and thus, this arrangement is not considered for further analysis. Although the segmented solid steel can be used for the rotor, it would not be beneficial compared to the milled/slitted arrangement. This is due to the single rotor body of the slitted arrangement which allows for increased stiffness of the shaft when compared to the segmented case. The milled single rotor body (see Fig.3b) is therefore analyzed with respect to optimizing the stack thickness and space in between.

Fig.5 shows the obtained maximum stress for different thicknesses of the slit space and associated slit thickness (1mm, 2mm, 5mm, 10mm, 15mm and 20mm). As can be seen

from Fig.5, the localized maximum stress in the rotor fluctuates with both the thickness of the steel and the space between them. It also can be seen that the obtained stresses for different stack thickness are lower at three regions. Those minimal stress regions are M1 (0.2mm – 0.4mm), M2 (0.65mm – 0.9mm) and M3 (2.4mm – 2.6mm). Region M3 has a comparatively larger distance between the stacks, but still shows low stresses. Region M1 is the optimal space distance for all the cases, however, this would be complex to produce due to the size of the wire and a limitation on manufacturing tools. Thus, a stack thickness between 2mm and 4mm and a space distance range from 0.2mm to 0.6mm are considered for further design optimization.

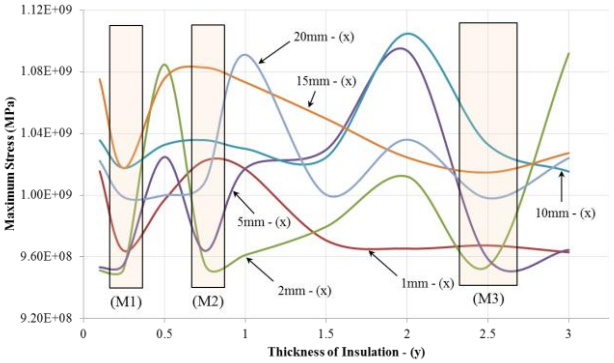

Fig. 5. Maximum stress induced in solid steel against the space between two stacks of solid steel. (M1, M2 and M3 are the regions of minima)

V. Rotor Design and Analysis

As previously mentioned, a high strength stainless steel (PH17-4) that has tensile strength of 1448MPa has been selected for the analysis. The active section of the rotor body is slitted or segmented so as to minimize eddy current losses. The magnet segments are then placed into the active section of the rotor body. To achieve better stress distribution on the rotor whilst satisfying the torque-speed requirement shown in Fig.1, the areas associated with the magnet, hollows, wedges and iron bridges (shown in Fig. 6a) are optimized. Both electromagnetic and structural optimizations are performed using Finite Element (FE) analysis.

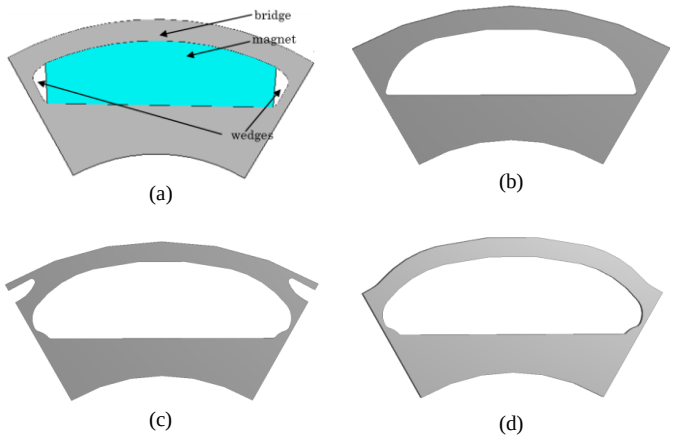

Fig. 6. Structural geometry adaptations considered in the optimization

A. Design optimization

The structural optimization of the rotor begins with an initial IPM rotor design based on the FE magnetic analysis. In the initial design, an analytical model [18] estimates the stresses due to the centrifugal forces that act on the bridges, by representing a ring equivalent to the mass of both the iron-bridge and the magnet. This is used along with FE electromagnetic analysis. The rotor is optimized considering the torque-speed requirement and then subject to a detailed coupled structural and magnetic FE analysis. At this stage, several design modifications are considered. The initially adopted rotor design is shown in Fig.6a and the considered alternative design adaptations are presented in Fig.6b-d.

Table I presents four different design cases to illustrate the influences of the structural adaptation on the rotor stress distribution. Geometry case - A represents the initial design (Fig.6a) considered and geometry cases - B1, B2 and B3 are modified geometry cases of Fig.6b. Associated stress plots for case – A and case - B3 are shown in Fig.7a and Fig.7b, respectively.

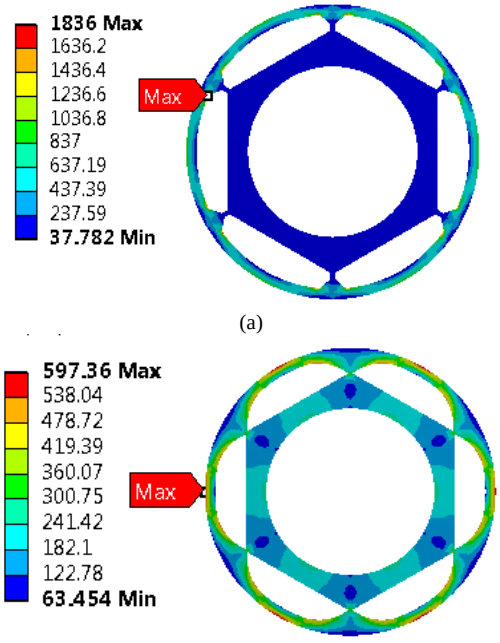

Fig. 7. Stress distribution (MPa) in the IPM rotor: (a) initial design (case–A) and (b) optimized first set design (case-B3) (Units are in MPa)

TABLE I
STRESS DISTRIBUTION FOR DIFFERENT STRUCTURAL ADAPTATIONS

Geometry Cases	A	B1	B2	B3
Rotor outer diameter (mm)	92	92	92	92
Magnet outer diameter (mm)	85.6	85.6	85.6	85.6
Round corner radius (mm)	0	5	10	15
Bridge thickness (mm)	3.22	3.22	3.22	3.22
Magnet cross sectional area (mm^2)	310.7	308.3	289	273.9
Magnet area reduction (%)	0	-1	-7	-12
Maximum stress (MPa)	1836	940	737	597
Maximum deformation (mm)	0.2	0.15	0.13	0.09
Starting torque reduction (% with respect to Case-A)	-	9.25	14.81	22.22

As can be seen from the results, although the geometry in case – A can provide the required magnetic performance, it experiences a high stress concentration localized at the edges (see Fig. 7a). Thus, a round corner is introduced to minimize the stress as explained in Table I. It is worth noting that the maximum stress is significantly reduced when 15mm radius round corner edges are adopted as shown in Fig.7b. Although the additional radius on the edges is beneficial for stress level reduction, the arrangement reduces the active magnet area; consequently, the magnetic performance is also altered. Given that the stress limit is lower than the yield strength of the material, either the bridge can be further reduced or the magnet area can be increased by increasing its depth to enhance the airgap flux density.

Table II shows a series of results obtained for various combinations of bridge thickness and magnet area. As expected the maximum stress is more sensitive to the bridge thickness than the magnet cross sectional area. In comparison with different cases considered in the study, Case - C7, while it experiences a maximum stress of 1100MPa with a safety factor of 1.32, fulfils the minimum safety factor set beforehand. Also, it is worth noting that amongst the arrangements (C1 to C7), only Case - C7 satisfies the starting torque requirements. Therefore, Case - C7 is investigated further, adopting the arrangements shown in Fig.6c and Fig.6d. The stress distributions obtained for these cases are presented in Fig.8. It is worth noting that by introducing an air slot (Case – C71), or removing material at the rotor outer periphery (Case – C72), the required torque at starting is achieved while stress distribution is not significantly altered. This can be seen in Fig. 8. Finally, Case- C72 is selected considering the slight reduction of maximum rotor stress.

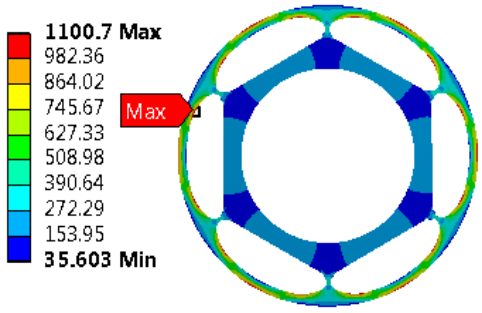

(a)

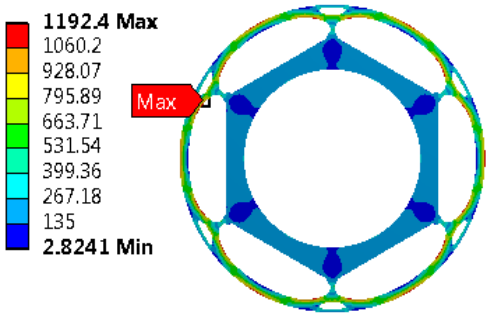

(b)

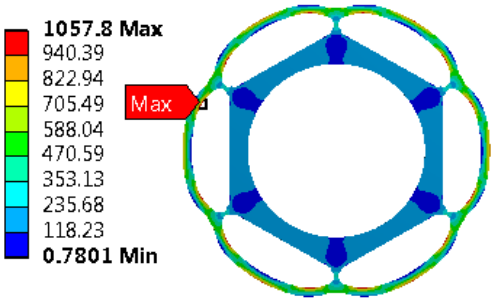

(c)

Fig. 8. Stress distribution in the IPM rotor: (a) Case – C7, (b) modified design with air slot (Case- C71) and (c) modified design with material reduction on the rotor surface (Case- C72) (Units are in MPa)

TABLE II
INFLUENCE OF THE BRIDGE THICKNESS AND MAGNET CROSS-SECTIONAL AREA ON ROTOR STRESS

Geometry cases	**C1**	**C2**	**C3**	**C4**	**C5**	**C6**	**C7**
Rotor outer diameter (mm)	92	92	92	92	92	92	92
Magnet outer diameter (mm)	86	86	86	87	87	88	86.5
Bridge thickness (mm)	3	3	3	2.5	2.5	2	2.75
Magnet distance from origin (mm)	33	32	31	33	32	33	32
Magnet cross sectional area (mm^2)	308	341	376	330	365	353	353
Magnet area reduction compared to case-A (%)	-1	10	21	6	18	14	14
Maximum stress (MPa)	767	757	869	978	1046	1318	1101
Maximum deformation (mm)	0.14	0.14	0.16	0.19	0.20	0.27	0.21
Safety factor	1.89	1.91	1.67	1.48	1.38	1.10	1.32

B. Eddy current loss analysis

Although the design is optimized to fulfill both magnetic and structural stress constraints, it is important to ensure that the losses generated in the rotor satisfy the thermal limit. The losses are therefore estimated for different arrangements of the following parameters: a different number of slits on the rotor body, the space between the slits and the slit depth. For the computation, 3D FE electromagnetic analysis is used. The resultant eddy current losses for different arrangements are gathered and analyzed. Obtained results are presented in Table III and Fig.9.

TABLE III
EDDY CURRENT LOSSES FOR DIFFERENT SLIT ARRANGEMENTS

Description	Eddy Current losses (W)
4mm sliced rotor, 26mm slit depth, space 0.2mm	333.89
4mm sliced rotor, 26mm slit depth, space 0.4mm	335.35
4mm sliced rotor, 26mm slit depth, space 0.6mm	335.69
4mm sliced rotor, 20mm slit depth, space 0.4mm	347.82
4mm sliced rotor, 15mm slit depth, space 0.4mm	507.60

From Table III, it is also clear that the space between the rotor slits has no influence on the induced eddy current losses. Conversely, the slit depth has significant influence, with losses reducing with increasing slit depth. This relationship is more apparent at shallower depths of slit; for example, the loss

difference between the slit depth of 20mm and 26mm for the considered rotor is less than 3.5%, while the difference between 15mm and 20mm is 31.5%. Therefore, implementing a minimal slit thickness allows improving the rotor stiffness and thus, operational speed.

From Fig.9, it can be seen that, as expected, the eddy current losses reduce with an increasing number of rotor silts. This is due to the reduction in the eddy current path which becomes smaller with an increasing number of slits. Selecting 57 slits - which provides the rotor with a slit thickness of 1mm - results in a ~17% (starting) torque reduction (for a given current loading), compared with a completely solid rotor. A rotor with 19 slits (4mm slice thickness) has a torque reduction of ~3%. However, torque can be improved if the slit space is kept minimal. It is worth noting that the key design limitation comes from manufacturing practicality, so a minimal space between slits of 0.2mm is selected based on current manufacturing feasibility.

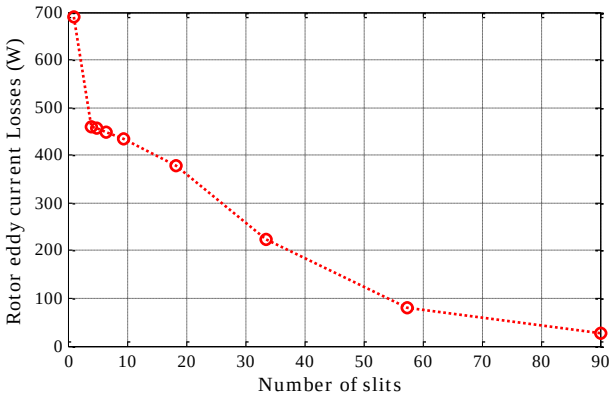

Fig. 9. Rotor iron eddy current losses vs. number of slits on the rotor

C. *Thermal analysis*

In order to ensure that the design is working within the operational temperature range, a thermal analysis is carried out for different slit thicknesses. In the design, the space between the slit and the slit depth are set to be 0.2mm and 20mm respectively. Due to the high power density requirements in the design, the machine is loaded with a high current density. Oil cooling is therefore adopted for the stator, in which the stator region is isolated from the rotor region and flooded with oil, allowing the rotor to run dry and maintain minimal windage losses. A lumped parameter thermal model is used to predict the thermal performance. For accuracy, a 1/6 cross-section of the rotor is modelled initially using Computational Fluid Dynamics (CFD) software with the predicted heat transfer coefficient later implemented in the lumped model. The detailed thermal analysis adopted for the design can be found in [24]. It is worth highlighting that the temperature should be limited within the rotor as the cooling is only available at the stator.

The obtained temperature distributions for 3mm slitted rotor are shown in Fig.10. A comparison of the results at slit thicknesses of 2, 3 and 4mm slitted rotors is presented in Table IV. From the results, it is obvious that the temperature - and therefore losses - varies as function of slit thickness. It is also worth noting that the temperature of the magnet (Recoma® grade 30S, Samarium Cobalt [25]) is lower than the magnet's maximum thermal limit (350°C). This confirms the design is thermally viable.

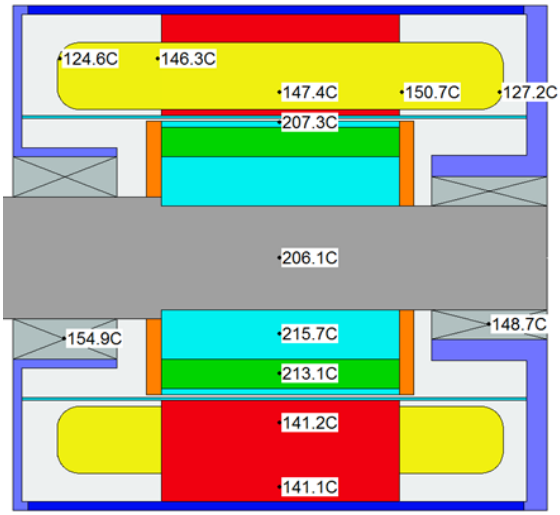

Fig. 10. Temperature distributions inside the 3mm slitted rotor machine

TABLE IV
TEMPERATURE COMPARISON BETWEEN DIFFERENT SLIT THICKNESSES

Location of temperature reading	2mm	3mm	4mm
Ambient (°C)	35	35	35
Housing (°C)	135.42	136.18	137.52
Stator back iron (°C)	140.52	141.12	142.19
Stator Surface (°C)	141.79	143.14	145.52
Rotor Surface (°C)	194.77	207.27	229.39
Magnet (°C)	199.25	213.07	237.52
Airgap Banding (°C)	194.99	207.56	229.8
Rotor back iron (°C)	201.12	215.72	241.55
Shaft (°C)	193.3	206.13	228.83
Winding Maximum (°C)	150.11	150.66	151.63

TABLE V
EFFECTS OF DEPTH OF SLITTING AND SPACE BETWEEN THE STACKS ON DYNAMIC PERFORMANCES OF ROTOR

	Bending modes	1st	2nd
	Natural frequencies	(Hz)	(Hz)
S1	Whole shaft no Magnets	2723.3	6343.5
S2	Whole shaft with Magnets	2562.9	4901.9
S3	3mm slits, 26mm slit depth, with magnets 0.2mm space	1656.5	1785.2
S4	4mm slits, 26mm slit depth, with magnets 0.2mm space	1948.3	2095.2
S5	4mm slits, 26mm slit depth, with magnets 0.4mm space	1975.0	2085.3
S6	4mm slits, 26mm slit depth, with magnets 0.6mm space	1951.5	2080.8
S7	4mm slits, 28.5mm slit depth, with magnets 0.4mm space	1781.7	2028.1
S8	4mm slits, 31mm slit depth, with magnets 0.4mm space	1538.9	1978.8

D. *Rotor dynamic analysis*

Since the rotor is slitted into several disks, the dynamic profile of the rotor is expected to change. Rotor dynamic analysis is therefore performed for both 3mm and 4mm slitted rotors, with different cases of slit depth, and compared with an unmodified whole rotor. The results obtained are listed in Table V.

From Table V, it is evident that while the mass of the magnet influences the natural frequencies, they are well above the operating speed of machine. Slicing the rotor decreases its stiffness and consequently reduces the natural frequencies as illustrated in Case - S2, Case – S3 and Case – S4. This effect is not large enough to change the mode shape of shaft as shown in Fig. 11. It is clear from the Fig.11 that the rotor shaft does affect the stiffness and reduces the natural frequencies with slit depth increases. Also it is evident here that there are no significant effects on rotor stiffness due to changes in space distance between the slits.

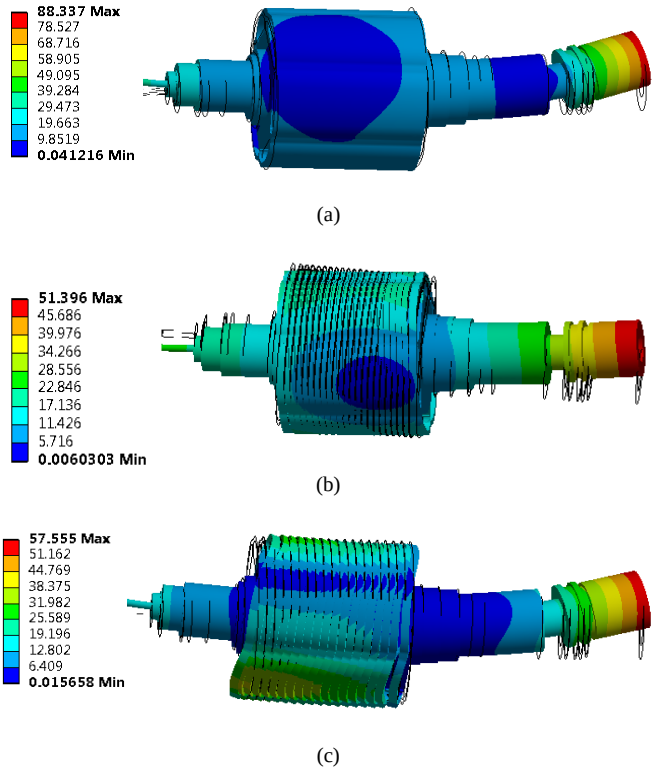

Fig. 11. Dynamic response of (a) solid rotor, (b) 3mm slitted rotor and (c) 4mm slitted rotor (S4) (Units are in mm)

Although the natural frequency of the design is higher than the operating speed, it is important to ensure that the bearing stiffness is sufficient. The design which has rotor shaft with 26mm slit depth and 0.4 mm space between the slits is therefore investigated by setting a bearing stiffness of 1E8 N/m at both shaft ends. Fig. 12 shows the obtained Campbell diagram for the considered bearing-rotor-shaft case. From the results, it can be seen that with a bearing stiffness of 1E8 N/m at both shaft ends, the critical speed is well below the natural frequency and thus, the rotor is stable.

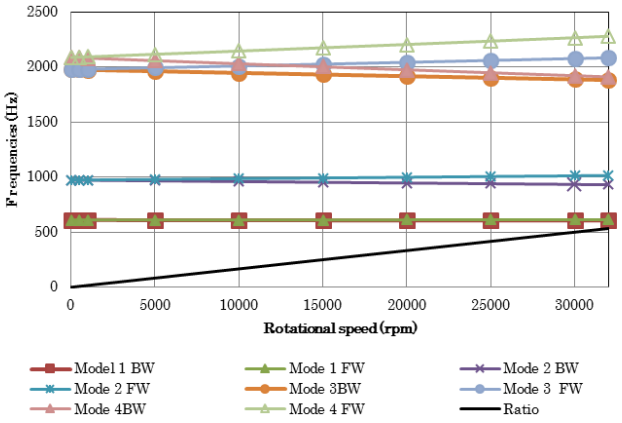

Fig. 12. Campbell diagram for the rotor with 0.4mm space between the stack and 26mm milling depth under bearing stiffness of 1E8N/m (Mode – Bending Mode; BW – Backward; FW – Forward)

In conclusion, the proposed solid rotor topology is feasible magnetically and structurally. The design is also thermally feasible if the rotor losses are minimal as expected. In section VI an experiment is carried out to verify the eddy current losses associated with the solid materials being considered for this application.

VI. Experimental Characterization of Solid Rotor

The key scope of this section is to evaluate the eddy current losses associated with the proposed slitted rotor in comparison with a solid rotor body. This allows confirming that the proposed slitted concept minimizes the losses and thus, the concept is thermally viable. Two different solid arrangements that have same dimensions (outer diameter, inner diameter and stack length) are adopted for the measurement. These are a complete solid body and a slitted body as shown in Fig.13. A representative stainless steel (grade 431) sample available in the laboratory is adopted for the test. The slitted body has 5 slits, 2mm wide and of 20mm depth from the outer surface of the rotor.

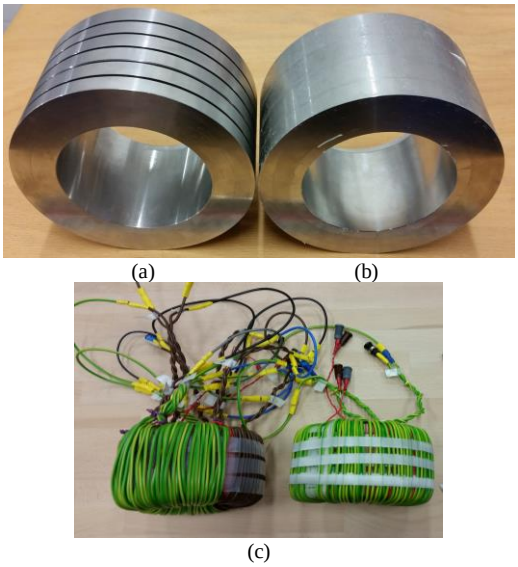

Fig. 13. Two different rotor arrangements: (a, b) slitted body and complete solid body and (c) prepared samples for testing

For the loss measurement, a state of art [26] testing facility that is available in-house was used. The setup specifications are shown in Table VI. It is worth noting that the operating temperatures depend on the furnace capability and not on the capability of the measurement facility. The actual pressure (MPa) applied to the samples is subject to the dimensions of those samples. The samples prepared for the measurement are shown in Fig. 13c where the test samples are wound using two windings, the primary and the secondary to magnetise the steel and the measure the dropped and induced voltage across the medium, respectively. Based on the gathered voltage and current data, the losses are estimated. The obtained losses are presented in Fig.14. The measurements are limited to the frequency of 50Hz, since the current (and consequently voltage) providing the flux density level in the sample is also limited. To test the samples at a higher frequency while maintaining the flux density level requires a larger supply than that which is available. However, the losses obtained at low frequency provide an indication of the loss reduction due to slitting.

TABLE VI
SPECIFICATIONS AND CAPABILITIES OF THE MEASUREMENT FACILITY

Parameter		Quantity
Fundamental Frequency		2 – 5000 Hz
Switching/Harmonic Frequency		5 – 40 kHz
Low Frequency Amplifier Capacity		100V 52 A (Peak)
		60V 40A (Continuous)
High Frequency Amplifier Capacity		50V 10A (Peak and continuous)
Operating Temperatures	Soft Magnetic Materials	-40ºC to 180ºC
	Hard Magnetic Materials	-40ºC to 300ºC
Operating force	Soft Magnetic Materials	0 – 3 kN (Compression / Tension)
	Hard Magnetic Materials	0 – 1kN (Compression)
Excitation Waveforms		Sine Wave
		DC / Normalized
		PWM
		Harmonic
		User Defined

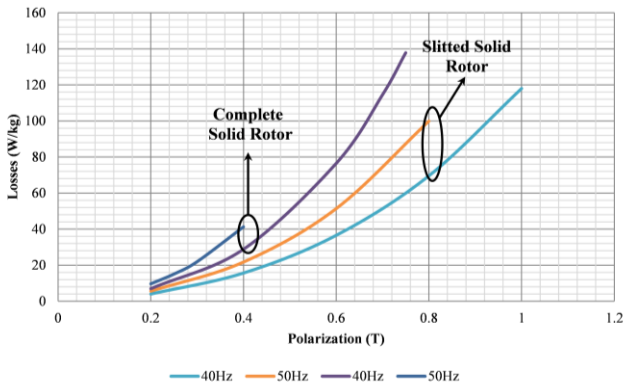

Fig. 14. Loss comparison of different rotors for 40Hz and 50Hz sinusoidal excitation

Fig. 14 shows the AC loss comparison between the solid body and slitted body for excitation frequencies of 40Hz and 50Hz. As expected there is a considerable reduction in the losses associated with the slitted body - an average reduction of 48% - compared to the complete solid body.

Table VII shows the estimated losses under load for the considered IPM machine with two different rotor arrangements (solid rotor and rotor with 5 slits) based on the measured material (stainless steel 431) loss data. From the results, it is evident that the losses associated to the slitted rotor are significantly lower than the complete solid rotor. This further confirms that the slitted rotor topology effectively minimizes the eddy current losses.

TABLE VII
LOSSES COMPARISON BETWEEN THE TWO DIFFERENT ROTOR ARRANGEMENTS

Type of body		**Solid rotor**	**Slitted rotor**
Predicted losses based on measurement at	30Hz	28.57 W	9.20W
	50Hz	46.62W	12.96W

VII. CONCLUSION

In this paper, a novel solid rotor topology which can cope with high structural stress has been proposed for IPM machines. The stress distributions and dynamic performances associated with such rotor concepts are analyzed using FE. An optimization study on IPM shape and the curvature angle has been done to improve the structural performance. To minimize the eddy current losses, a partly slitted solid rotor which shorts the eddy current paths has been investigated. It was shown that the depth of slit has to be limited because of the reduction in both stiffness and natural frequency with an increase in slit depth. It was also shown that space between the rotor slices does not have any influence on rotor stiffness, and is only limited by the manufacturability of such design. Eddy current analysis confirmed that the losses are a function of the thickness of the rotor slices and a trade-off between the performance and the losses is required. It was also shown that the design is thermally viable and that it is important to reduce the rotor losses to a minimum in order to maintain the temperature within limits, by taking into account available cooling. The results obtained from the two tested stainless steel samples - solid rotor construction and a slitted arrangement - further confirmed that the proposed slitted approach reduces the eddy current losses significantly and thus, the topology can effectively be implemented within the IPM machine.

REFERENCES

[1] B. Mecrow, J. Cullen, and P. Mellor, "Editorial - Electrical machines and drives for the more electric aircraft," *Electric Power Applications, IET*, vol. 5, pp. 1-2, 2011.

[2] A. Boglietti, A. Cavagnino, A. Tenconi, and S. Vaschetto, "The safety critical electric machines and drives in the more electric aircraft: A survey," in *Industrial Electronics, 2009. IECON '09. 35th Annual Conference of IEEE*, 2009, pp. 2587-2594.

[3] L. Chunhua, K. T. Chau, and Z. Xiaodong, "An Efficient Wind-Photovoltaic Hybrid Generation System Using Doubly Excited Permanent-Magnet Brushless Machine," *Industrial Electronics, IEEE Transactions on*, vol. 57, pp. 831-839, 2010.

[4] A. Di Gerlando, G. Foglia, M. F. Iacchetti, and R. Perini, "Axial Flux PM Machines With Concentrated Armature Windings: Design Analysis and Test Validation of Wind Energy Generators," *Industrial Electronics, IEEE Transactions on*, vol. 58, pp. 3795-3805, 2011.
[5] M. Pinilla, "Performance Improvement in a Renewable Energy Direct Drive Permanent Magnet Machine by means of Soft Magnetic Composite Interpoles," *Energy Conversion, IEEE Transactions on*, vol. 27, pp. 440-448, 2012.
[6] P. Arumugam, T. Hamiti, C. Brunson, and C. Gerada, "Analysis of Vertical Strip Wound Fault-Tolerant Permanent Magnet Synchronous Machines," *Industrial Electronics, IEEE Transactions on*, vol. 61, pp. 1158-1168, 2014.
[7] J. Xuefeng, H. Wenxin, C. Ruiwu, H. Zhenyang, and J. Wen, "Electric Drive System of Dual-Winding Fault-Tolerant Permanent-Magnet Motor for Aerospace Applications," *Industrial Electronics, IEEE Transactions on*, vol. 62, pp. 7322-7330, 2015.
[8] B. K. Bose and P. M. Szczesny, "A microcomputer-based control and simulation of an advanced IPM synchronous machine drive system for electric vehicle propulsion," *Industrial Electronics, IEEE Transactions on*, vol. 35, pp. 547-559, 1988.
[9] A. Choudhury, P. Pillay and S. S. Williamson, "Modified DC-link voltage balancing algorithm for a 3-level neutral point clamped (NPC) traction inverter based electric vehicle PMSM drive,"*Industrial Electronics Society, IECON 2013 - 39th Annual Conference of the IEEE*, Vienna, 2013, pp. 4660-4665.
[10] S. Shinn-Ming and P. Ching-Tsai, "Voltage-Constraint-Tracking-Based Field-Weakening Control of IPM Synchronous Motor Drives," *Industrial Electronics, IEEE Transactions on*, vol. 55, pp. 340-347, 2008.
[11] J. Sung-Yoon, C. C. Mi, and N. Kwanghee, "Torque Control of IPMSM in the Field-Weakening Region With Improved DC-Link Voltage Utilization," *Industrial Electronics, IEEE Transactions on*, vol. 62, pp. 3380-3387, 2015.
[12] S. Tianfu and W. Jiabin, "Extension of Virtual-Signal-Injection-Based MTPA Control for Interior Permanent-Magnet Synchronous Machine Drives Into the Field-Weakening Region," *Industrial Electronics, IEEE Transactions on*, vol. 62, pp. 6809-6817, 2015.
[13] E. Al-nabi, W. Bin, N. R. Zargari, and V. Sood, "Sensorless Control of CSC-Fed IPM Machine for Zero- and Low-Speed Operations Using Pulsating HFI Method," *Industrial Electronics, IEEE Transactions on*, vol. 60, pp. 1711-1723, 2013.
[14] D. Dorrell, L. Parsa, and I. Boldea, "Automotive Electric Motors, Generators, and Actuator Drive Systems With Reduced or No Permanent Magnets and Innovative Design Concepts," *Industrial Electronics, IEEE Transactions on*, vol. 61, pp. 5693-5695, 2014.
[15] A. M. El-Refaie, "Fractional-Slot Concentrated-Windings Synchronous Permanent Magnet Machines: Opportunities and Challenges," *Industrial Electronics, IEEE Transactions on*, vol. 57, pp. 107-121, 2010.
[16] R. Ni, D. Xu, G. Wang, X. Gui, G. Zhang, H. Zhan, *et al.*, "Efficiency Enhancement of General AC Drive System by Remanufacturing Induction Motor with Interior Permanent Magnet Rotor," *Industrial Electronics, IEEE Transactions on*, vol. PP, pp. 1-1, 2015.
[17] M. N. Uddin and M. Azizur Rahman, "High-Speed Control of IPMSM Drives Using Improved Fuzzy Logic Algorithms," *Industrial Electronics, IEEE Transactions on*, vol. 54, pp. 190-199, 2007.
[18] P. Arumugam, J. Dusek, A. Aigbomian, G. Vakil, S. Bozhko, T. Hamiti, *et al.*, "Comparative design analysis of Permanent Magnet rotor topologies for an aircraft starter-generator," in *Intelligent Energy and Power Systems (IEPS), 2014 IEEE International Conference on*, 2014, pp. 273-278.
[19] M. Barcaro, G. Meneghetti, and N. Bianchi, "Structural Analysis of the Interior PM Rotor Considering Both Static and Fatigue Loading," *Industry Applications, IEEE Transactions on*, vol. 50, pp. 253-260, 2014.
[20] B. Kou, C. Li, and S. Cheng, "Flux-Weakening-Characteristic Analysis of a New Permanent-Magnet Synchronous Motor Used for Electric Vehicles," *Plasma Science, IEEE Transactions on*, vol. 39, pp. 511-515, 2011.
[21] C. Zuhou, "Variable excitation permanent magnet synchronous motor.", http://www.google.com.gt/patents/CN102170211A?cl=en, Aug 2011, Google Patents, CN Patent App. CN 201,110,109,156.
[22] A. Tessarolo, M. Mezzarobba, and R. Menis, "A novel interior permanent magnet motor design with a self-activated flux-weakening device for automotive applications," in *Electrical Machines (ICEM), 2012 XXth International Conference on*, 2012, pp. 2603-2609.
[23] M. S. K. Hochhalter, "Permanent magnet motor or actuator with field weakening capability," Patent 20100213779, August 2010.
[24] Z. Xu, A. L. Rocca, S. J. Pickering, C. Eastwick, C. Gerada, and S. Bozhko, "Mechanical and thermal design of an aeroengine starter/generator," in *2015 IEEE International Electric Machines & Drives Conference (IEMDC)*, 2015, pp. 1607-1613.
[25] *RECOMA® Samarium Cobalt Magnets, ARNOLD Magnetic Tecnologies*. Available: http://www.arnoldmagnetics .com/Portals/0/Files/RECOMA/Recoma%20Combined%20-%20160301.pdf?ver=2016-03-01-134105-057.
[26] W. Soong, "Bh curve and iron loss measurements for magnetic materials," *Power Engineering Briefing Note Series*, 2008.

Puvan Arumugam (M'11) received the B.Eng. (Hons.) degree in electrical and electronic engineering from The University of Nottingham, Nottingham, U.K., in 2009, and the Ph.D. degree in electrical machines and drives from The University of Nottingham, Nottingham, U.K., in 2013. He subsequently worked as a researcher within the Power Electronics, Machines, and Control Group, The University of Nottingham, working on electric aircraft propulsion. He is currently a Senior Project Engineer with the Force Engineering Ltd, Shepshed, UK.

His current research interests include electrical machines and drives, electromechanical devices and systems, and analytical computation of electromagnetic fields. In 2014, Dr. Arumugam was awarded a Hermes Fellowship supported by Technology Transfer Office, The University of Nottingham.

Zeyuan Xu obtained his PhD in in Mechanical Engineering from the University of Manchester, UK, in 2002. He subsequently worked as a researcher at UMIST, Brunel University and University of Nottingham. His main research interests are in turbulent thermos-fluid flow, heat transfer enhancement, thermal management of advance electrical motor and power electronics, and mechanical design of high speed electrical machine.

Antonino La Rocca obtained his PhD in Mechanical Engineering from the University of Nottingham, UK, in 2016; received his BEng and MEng in Mechanical Engineering from the University of Palermo in 2010 and 2011 respectively. He is currently working as researcher in the Fluids and Thermal Engineering research group. His research is mainly focused on fluid-dynamics, heat transfer and analytical and numerical thermal modelling of electrical machines.

Gaurang Vakil received the B.E. degree in electrical engineering from the Saurashtra University in 2006 and M. Tech. with Gold Medal from the Nirma University in 2008. He is currently working toward completion of the Ph.D. degree in variable speed generator design for renewable energy applications with the Power Electronics, Machines and Drives (PEMD) group at Indian Institute of Technology - Delhi (IITD). He is also working as a Research Associate with Power Electronics, Machines and Controls (PEMC) group at the University of Nottingham. His main research interests are analytical modelling and design optimization of electrical machines, optimizing electric drive-train for pure electric and hybrid vehicles, high power density machines, magnetic material characterization and high-performance electrical machines for transport, traction and renewable energy applications.

Matthew Dickinson received a B.Eng. (Hons.) degree in Mechanical Engineering from De Montfort University, Leicester, U.K. in 2008. He is working as a project engineer at Force Engineering Ltd., Leicestershire, UK, where he is involved in the thermal and mechanical design of Linear Motors. His main research interests include thermal management, analytical computational tools for Linear Motors, and advanced materials for electrical machines.

Emmanuel Amankwah received the BSc degree in Electrical & Electronic Engineering from KNUST (2006), Ghana and the MSc and PhD degrees in Electrical engineering (2009) and Electrical & Electronic Engineering (2013), respectively, from The University of Nottingham, Nottingham, U.K. Between 2006 and 2008 Emmanuel worked with the Electricity Company of Ghana as a design Engineer. Since 2013, he has being working as a Research Fellow in emerging technologies for HVDC power transmission at the Power Electronic Machines and Control research group (PEMC) at the University of Nottingham, Faculty of Engineering, Nottingham. His main research activities are in power electronics for grid integration and has interest in motor drive control.

Tahar Hamiti was born in Larbàa Nath Irathen, Algeria, in 1979. He received the Ingénieur d'Etat degree in automatic control systems from the University of Tizi-Ouzou, Tizi-Ouzou, Algeria, and the Ph.D. degree in electrical engineering from the University of Nancy I, Nancy, France. From 2010 to 2015, he was a Research Fellow and subsequently a Lecturer within the Power Electronics, Machines and Control Group, The University of Nottingham, UK.

In 2015 Dr Hamiti joined VEDECOM, a French institute for energy transition to work on novel electrical machines for electric and hybrid vehicles. His research interests include modeling, optimal design, and control of high-performance electrical machines for transportation applications and power generation.

Serhiy Bozhko (M'96) received the M.Sc. and Ph.D. degrees in electromechanical systems from the National Technical University of Ukraine, Kyiv city, Ukraine, in 1987 and 1994, respectively. Since 2000, he has been with the Power Electronics, Machines and Controls Research Group of the University of Nottingham, Nottingham, U.K. Serhiy has been a Principal Research Fellow and is currently an Associate Professor in Aircraft Electrical Systems. He has been involved in leading several EU- and industry-funded projects in the area of aircraft electric power systems, including control and stability issues, power management, as well as advanced modeling and simulations methods.

Chris Gerada (M'05) received the Ph.D. degree in numerical modeling of electrical machines from The University of Nottingham, Nottingham, U.K., in 2005. He was subsequently a researcher with The University of Nottingham, where he was involved in high-performance electrical drives and the design and modeling of electromagnetic actuators for aerospace applications. Since 2006, he has been the Project Manager of the GE Aviation Strategic Partnership. In 2008, he was appointed as a Lecturer in electrical machines, an Associate Professor in 2011, and a Professor with The University of Nottingham, in 2013.

His current research interests include the design and modeling of high-performance electric drives and machines. He serves as an Associate Editor of the IEEE Transactions On Industry Applications and is the Chair of the IEEE Industrial Electronics Society Electrical Machines Committee.

Stephen J. Pickering received the B.Sc. and Ph.D. degrees in mechanical engineering from the University of Nottingham, Nottingham, U.K., in 1979 and 1984, respectively. He joined the University of Nottingham as a lecturer in 1988, where he is currently Hives Professor of Mechanical Engineering in the Faculty of Engineering. He has extensive research experience in thermos-fluids and has undertaken research into the cooling of electric machines for over twenty years.